Shell structure of Ti and Cr nuclei from measurements of g factors and lifetimes

R. Ernst,[1] K.-H. Speidel,[1] O. Kenn,[1] A. Gohla,[1] U. Nachum,[1] J. Gerber,[2] P. Maier-Komor,[3] N. Benczer-Koller,[4] G. Kumbartzki,[4] G. Jakob,[4] L. Zamick,[4] and F. Nowacki[5]

[1]*Institut für Strahlen- und Kernphysik, Universität Bonn, Nußallee 14-16, D-53115 Bonn, Germany*

[2]*Institut de Recherches Subatomiques, F-67037 Strasbourg, France*

[3]*Physik-Department, Technische Universität München, James-Franck-Strasse, D-85748 Garching, Germany*

[4]*Department of Physics and Astronomy, Rutgers University, New Brunswick, New Jersey 08903*

[5]*Laboratoire de Physique Théorique, 3-5 rue de l'Université, 67084 Strasbourg Cedex, France*

(Received 18 February 2000; published 10 July 2000)

g factors and lifetimes have been measured for the first 2^+ and 4^+ states of ^{46,48}Ti and ^{50,52}Cr employing the combined technique of projectile Coulomb excitation and transient magnetic fields. The same target was used in all measurements. The individual isotopes were provided by the ion source of the accelerator. These conditions guarantee high reliability and precision as demonstrated in earlier experiments. While the global behavior of the data is well explained by full fp shell model calculations, distinct deviations from theoretical predictions for ^{46,48}Ti might be attributed to excitations of the ^{40}Ca core.

PACS number(s): 21.10.Ky, 25.70.De, 27.50.+e

I. INTRODUCTION

Magnetic moments and lifetimes of nuclear states are sensitive to the detailed composition of nuclear wave functions. Since the spin g factors of protons and neutrons are different in sign and magnitude [$g_s(p)=+5.586$, $g_s(n)=-3.826$], magnetic moment measurements enable the determination of the proton or neutron nature of particular nuclear states. This unique feature has been well known for many years and has been dramatically displayed recently in g factor measurements for Nd [1] and Zr [2] isotopes near shell closures at $N=82$ and $N=50$. In order to test nuclear models and to distinguish between different predictions, g factors must be determined with a precision comparable to that achieved in recent measurements on Se isotopes [3]. The major purpose of the present experiments was to determine precise g factors and lifetimes of excited states of four fp shell nuclei, namely ^{46,48}Ti and ^{50,52}Cr close to shell closures at $Z=20$ and $N=28$. Comparisons with the results of the full fp shell model calculations provide stringent tests of the effective nucleon–nucleon interaction as well as of the model space used. The essence of these investigations has already been reported [4]; the present paper presents the details of the experiment and the results of the shell model calculations.

In this experiment, the g factors of the first 2^+ states were determined with much higher accuracy than obtained previously [5,6]. The g factors of the 4_1^+ states, with the exception of $g(4_1^+;{}^{50}\mathrm{Cr})$, were determined for the first time. In the case of ^{50}Cr, g factors of the 2^+ to 8^+ states had been measured previously with a fusion evaporation reaction [6]. In this experiment, all g factors were found to be practically the same (within their errors) contrary to microscopic calculations [7,8] which predict large variations as a function of spin. It was therefore important to remeasure the g factors of the 2_1^+ and 4_1^+ states in ^{50}Cr which, according to theory, should differ by a factor of 1.4 [7]. This goal was achieved by the use of projectile Coulomb excitation in inverse kinematics in combination with the technique of transient magnetic fields [3,9]. This new approach has been developed over the last 5 years and provides, for the first time, precise and reliable data. The merits of this experimental method consist in Coulomb exciting heavy projectiles by lighter target nuclei. γ rays are recorded in coincidence with the forward scattered target nuclei detected in a Si particle detector placed at 0° with respect to the beam axis. The technique provides kinematic focusing of the scattered projectiles. The high velocities of projectile nuclei traversing a polarized ferromagnetic foil result in large transient hyperfine magnetic fields at the nucleus of the moving ion. Moreover, the same target can be used for several different projectiles in the same mass region, obviating systematic errors arising from the use of different targets in the conventional technique of target excitation.

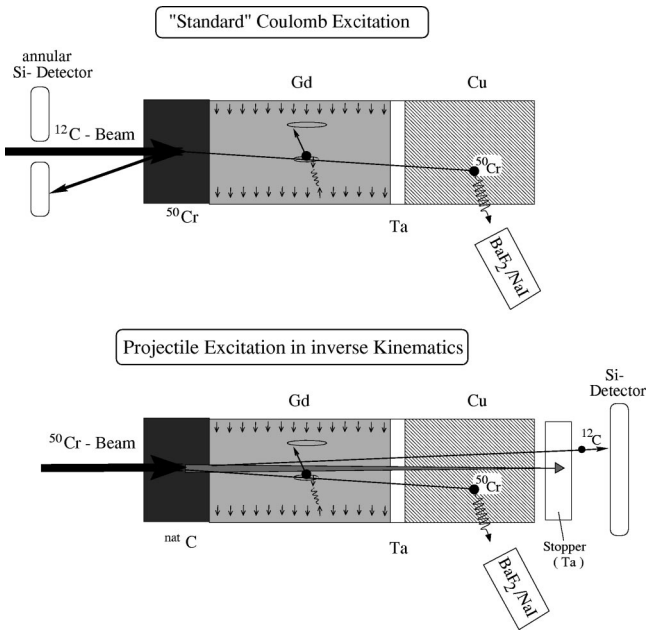

FIG. 1. Comparison of the targets used with (a) the standard technique for target Coulomb excitation and (b) projectile excitation in inverse kinematics.

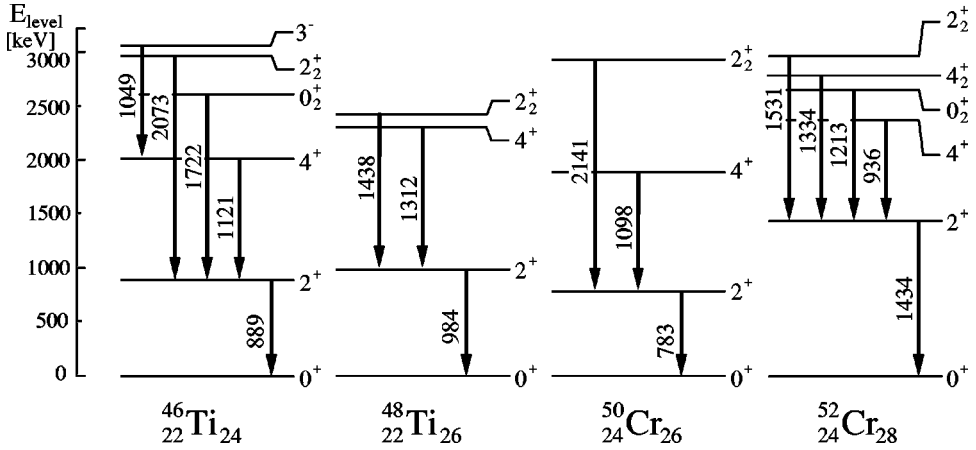

FIG. 2. Low-lying states of ^{46,48}Ti and ^{50,52}Cr.

These characteristics exhibit the further advantage of being appropriate for future experiments with low intensity beams of radioactive nuclei. Figure 1 shows a schematic of the experimental apparatus used in both the conventional method and inverse kinematics approach.

II. EXPERIMENTAL DETAILS

In the present experiments, beams of isotopically pure ^{46}Ti, ^{48}Ti, ^{50}Cr, and ^{52}Cr were provided by the ion source of the tandem accelerators at Cologne and Munich with intensities of about 1 pnA and energies between 110 and 120 MeV. The multilayer target consisted of 0.75 mg/cm^2 ^{nat}C layer deposited on a 3.6 mg/cm^2 gadolinium layer evaporated at 800 K on a 1 mg/cm^2 thick tantalum foil [10]; the tantalum was backed by a 3.6 mg/cm^2 copper layer to provide good thermal conductivity. The beam ions were Coulomb excited by the C to the 2_1^+, 4_1^+, and 2_2^+ states (Fig. 2) and subsequently traversed the ferromagnetic gadolinium layer in which they experienced spin precession in the transient hyperfine magnetic field. Finally, the excited ions traversed the tantalum layer and were stopped in the hyperfine interaction free copper layer. The target was cooled to liquid nitrogen temperature and magnetized to saturation by an external field of 0.06 Tesla. The high energy γ rays from the deexcitation of the ^{12}C($2^+ \rightarrow 0^+$; 4.43 MeV) target nuclei were weak and, therefore, contributed only a negligible background in the energy region of interest.

The γ rays emitted from the excited states of interest were measured in coincidence with the carbon ions using 12.7 cm $\times$ 12.7 cm NaI(Tl) as well as 9 cm $\times$ 9 cm BaF_2 scintillators. In some measurements, the superior time resolution of BaF_2 was used to discriminate γ rays from fusion reactions associated with light particle emission, whereas in other cases, the better energy resolution of NaI(Tl) scintillators was essential. In addition, an *n*-type, coaxial Ge detector with a relative efficiency of 40% was placed at 0° to the beam direction and served as monitor for contaminant lines and for the measurement of nuclear lifetimes via the Doppler shift attenuation method (DSAM). Figure 3 shows a coincidence spectrum of the Ge detector.

The high beam energies required for an efficient excitation of the 4_1^+ states produce fusion reactions with the ^{12}C target and result in additional features in the spectra. The following reactions, in which nuclei were produced whose γ lines could not be resolved by the scintillators, were particularly strong: ^{12}C(^{46,48}Ti,2α)^{50,52}Cr and ^{12}C(^{50,52}Cr, 2α)^{54,56}Fe. This problem, however, could be solved in two ways. First, the excellent time resolution of the BaF_2 scintillators enabled the separation of Coulomb excitation events associated with carbon ions from those with charged particle reactions, as shown in a three-dimensional energy-versus-time plot for ^{50}Cr (Fig. 4). Second, by operating the 100 μm Si detector at a very low bias ($\simeq$10 V), the light particles do not deposit their whole energy in the active part of the detector, and can, therefore, be separated from carbon ions (Fig. 5). By gating only on the carbon ions, no γ lines from the charged particle reactions contributed to the spectra. NaI(Tl) scintillators were used for ^{46}Ti since the better energy resolution was required to separate the close lying γ lines of the ($4_1^+ \rightarrow 2_1^+$) and ($3_1^- \rightarrow 4_1^+$) transitions (see Fig.

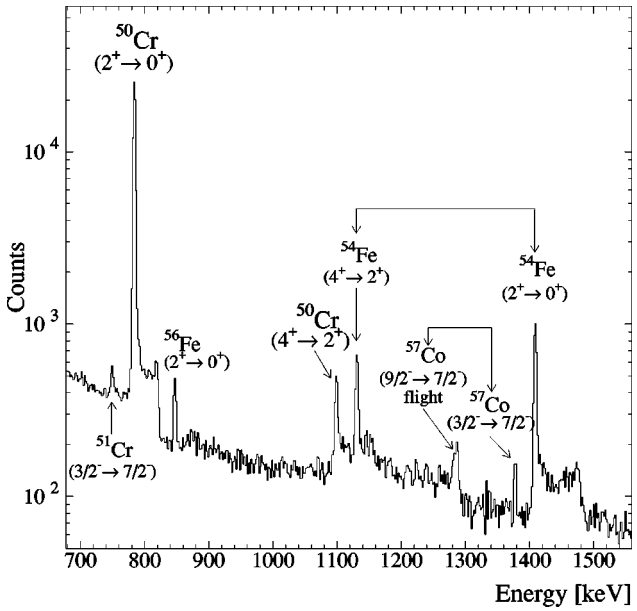

FIG. 3. Ge coincidence spectrum at 0° showing the Coulomb excited ($2_1^+ \rightarrow 0_1^+$) and ($4_1^+ \rightarrow 2_1^+$) transitions of ^{50}Cr as well as γ-ray lines of nuclei produced in charged particle reactions with ^{12}C. The ^{12}C(^{50}Cr,2α)^{54}Fe reaction was particularly strong.

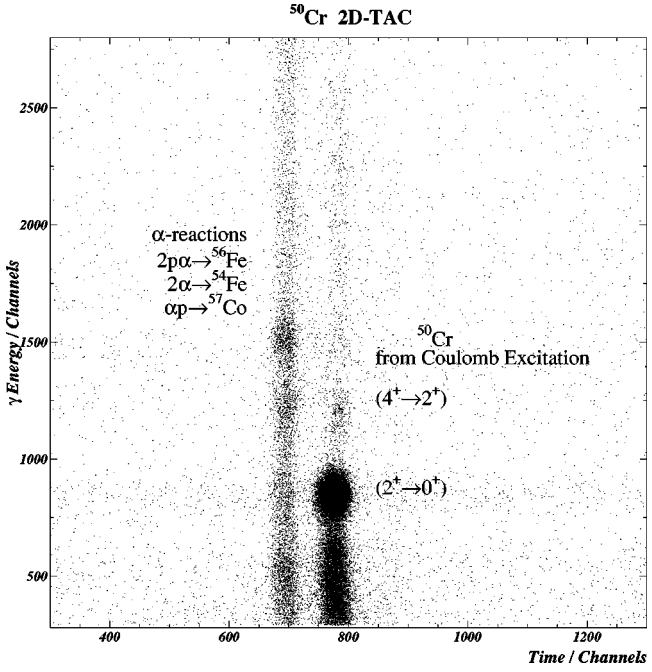

FIG. 4. Three-dimensional plot of γ-energy versus time for BaF_2 scintillators. The events resulting from Coulomb excitation are well separated from light particle events (mainly α particles) associated with fusion reactions.

2), whereas for ^{50}Cr and ^{52}Cr, BaF_2 detectors were sufficient (Fig. 6).

Another difficulty arose in the experiment on ^{48}Ti, which was first recognized in the Ge detector spectrum. A strong γ line at 1381.7 keV (Fig. 7) was identified and attributed to the ^{49}Ti $(3/2^- \rightarrow 7/2^-)$ transition. ^{49}Ti is produced by a one

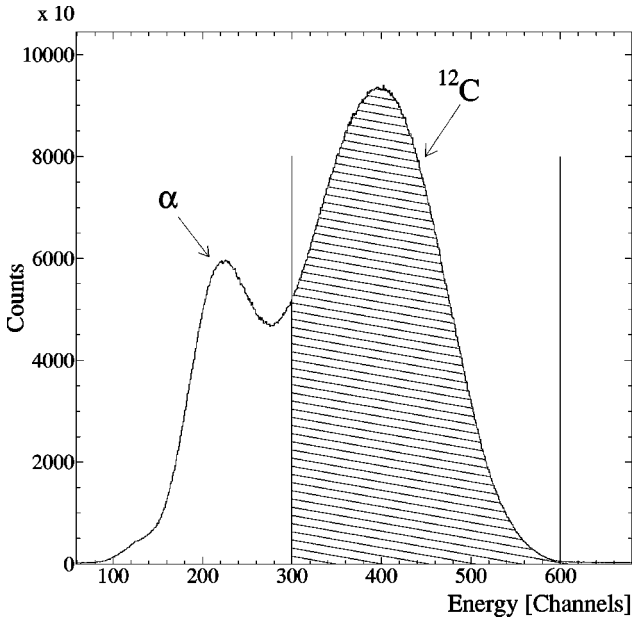

FIG. 5. Particle spectrum with a 100 μm Si detector at low bias. The α particles are well separated from carbon ions due to incomplete stopping. The shaded area corresponds to the gate conditions for the γ-coincidence spectra.

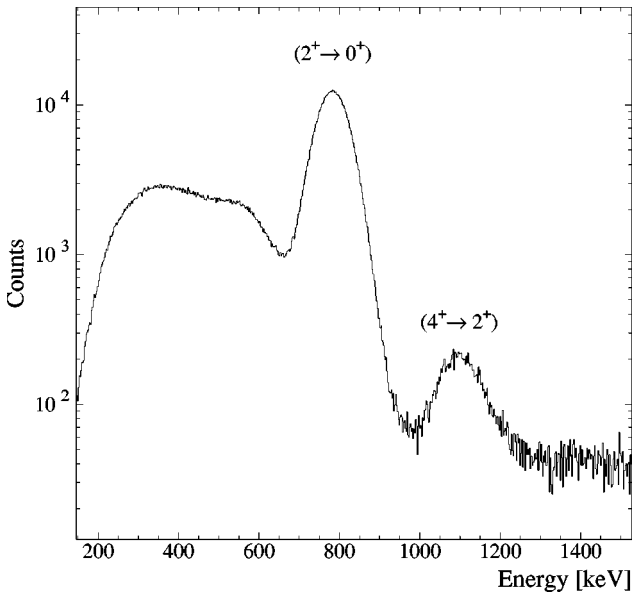

FIG. 6. BaF_2 γ-ray coincidence spectrum at 65° displaying well separated $(2_1^+ \rightarrow 0_1^+)$ and $(4_1^+ \rightarrow 2_1^+)$ transitions in ^{50}Cr.

neutron transfer reaction. Since the resulting nucleus, ^{11}C, could not be distinguished from ^{12}C ions, this γ line was unavoidable and could not be resolved from the ^{48}Ti$(4_1^+ \rightarrow 2_1^+)$ transition in the scintillator spectra. However, by increasing the beam energy to 115 MeV the line intensity was drastically reduced to a 5% level relative to the $(4_1^+ \rightarrow 2_1^+)$ photopeak intensity as shown in Fig. 7. Moreover, for resolving the $(4_1^+ \rightarrow 2_1^+)$ γ ray from the $(2_2^+ \rightarrow 2_1^+)$ γ ray, the better energy resolution of NaI(Tl) compared to BaF_2 was

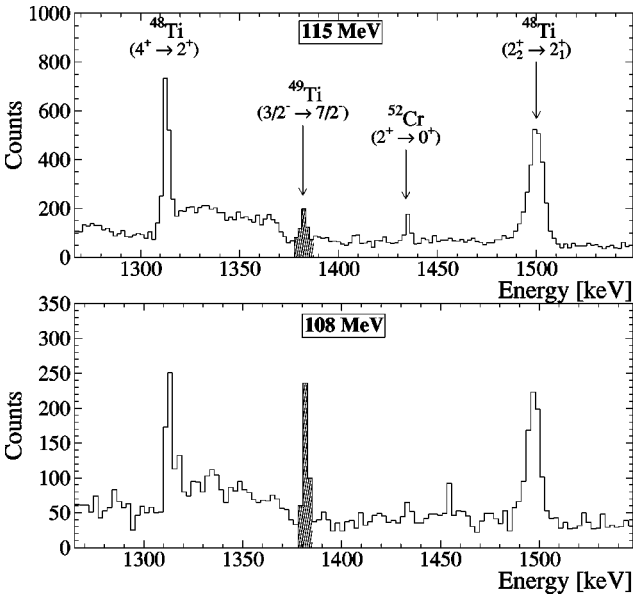

FIG. 7. Ge coincidence spectra at different beam energies. The intensity of the transition in ^{49}Ti produced by a one-neutron transfer reaction is drastically reduced at the higher energy. The line shapes of the $(4_1^+ \rightarrow 2_1^+)$ transition and the fully Doppler shifted $(2_2^+ \rightarrow 2_1^+)$ γ-ray lines of ^{48}Ti are clearly separated.

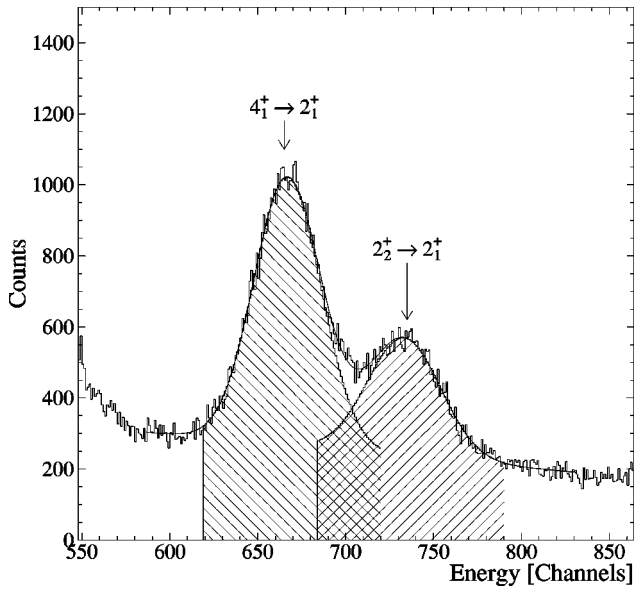

FIG. 8. NaI(Tl) spectrum of the transitions in ^{48}Ti. The $(4_1^+ \rightarrow 2_1^+)$ and the Doppler shifted $(2_2^+ \rightarrow 2_1^+)$ transitions at $\theta_\gamma = 115°$ are well resolved.

used to determine the intensity of the $(4_1^+ \rightarrow 2_1^+)$ transition. The separation of the two γ rays was further diminished for the detectors at backward angles, as the $(2_2^+ \rightarrow 2_1^+)$ γ ray was fully Doppler shifted due to the short lifetime of the 2_2^+ state (Fig. 8 and Table II).

The particle-γ angular correlation is given by [11,12]

$$W(\theta_\gamma) = 1 + \sum_{k=2,4} A_k^{\text{expt}} P_k(\cos(\theta_\gamma)), \tag{1}$$

where $A_k^{\text{expt}} = G_k Q_k A_k^{\text{th}}$ and A_k^{th} are the experimental and theoretical coefficients, respectively. The coefficients A_k^{th} correspond to the case of maximum alignment of the nuclear spin perpendicular to the beam axis. P_k are Legendre polynomials. The coefficients Q_k represent an attenuation of the correlation due to the finite size of the γ-ray detectors [13], while G_k represents, the attenuation resulting from the finite acceptance angle of the particle detector. The factor G_k has been treated in great detail for the case of loss of alignment due to the influence of extranuclear fields [11,12] . In the case of loss of alignment resulting from the finite solid angle subtended by the particle detector, G_k takes the form $G_k = 1 - Q \cdot k(k+1)$, for small Q [13,14]. Thus, there remains only one unknown parameter, Q, which is required to determine the coefficients A_k^{expt}. The value of this parameter was obtained from the measurement of the anisotropy R,

$$R = \sqrt{\frac{N_i(+50°) \cdot N_j(-50°)}{N_i(+80°) \cdot N_j(-80°)}}, \qquad R = \sqrt{\frac{N_i(+130°) \cdot N_j(-130°)}{N_i(+100°) \cdot N_j(-100°)}}, \tag{2}$$

where the γ-ray detectors were alternately placed at angles $\pm 50°$, $\pm 80°$, $\pm 100°$, and $\pm 130°$, and $N_{i,j}$ are the coincidence counting rates of the photopeak of the γ-ray transition in the ith and jth detector, respectively.

The logarithmic slope, $S(\theta_\gamma) = [1/W(\theta_\gamma)] \cdot [dW(\theta_\gamma)/d\theta_\gamma]$, is derived from the resulting angular correlation $W(\theta_\gamma)$. The slopes $S(\theta_\gamma)$, calculated in the rest frame of the γ-emitting nuclei at the angle θ_γ at which the spin precession measurements were carried out, are shown in Table I.

Precession angles Φ were derived from double ratios $DR = (N_i\uparrow \cdot N_j\downarrow)/(N_i\downarrow \cdot N_j\uparrow)$ of counting rates N with an external magnetic field alternately applied in ''up'' $(\uparrow)$ and ''down'' $(\downarrow)$ direction perpendicular to the γ-ray detection plane. The indices i,j represent a pair of γ detectors symmetric to the beam axis. The precession angles Φ are given by [15]:

$$\Phi^{\text{expt}} = \frac{1}{S} \cdot \frac{\sqrt{DR} - 1}{\sqrt{DR} + 1} = g \cdot \frac{\mu_N}{\hbar} \int_{t_{\text{in}}}^{t_{\text{out}}} B_{\text{TF}}(v_{\text{ion}}(t)) \cdot e^{-t/\tau} dt, \tag{3}$$

TABLE I. Summary of the average velocities of the ions entering, exiting, and traversing the ferromagnetic foil, the slopes of the angular correlations $S(\theta_\gamma)$, the measured angular precessions, and the expected precessions, Φ^{lin}/g, calculated from Eqs. (3)–(5) based on the linear parametrization of the transient field.

Nucleus	State	$\langle v/v_0 \rangle_{\text{in}}$	$\langle v/v_0 \rangle_{\text{out}}$	$\langle v_{\text{ion}}/v_0 \rangle$	$\lvert S(\theta_\gamma = 65°) \rvert$	Φ^{expt} (mrad)	Φ^{lin}/g (mrad)
^{46}Ti	2_1^+	4.5	1.2	2.5	2.158 (26)	14.56 (35)	29.34 (141)
	4_1^+				0.769 (84)	14.56 (426)	25.07 (121)
^{48}Ti	2_1^+	5.1	1.8	3.2	2.230 (5)	11.42 (14)	29.17 (141)
	4_1^+				0.951 (63)	12.29 (281)	22.61 (109)
^{50}Cr	2_1^+	4.9	1.6	3.0	2.275 (29)	21.04 (33)	33.97 (164)
	4_1^+				0.765 (43)	24.00 (391)	30.93 (149)
^{52}Cr	2_1^+	5.1	2.0	3.5	2.387 (39)	28.60 (66)	23.72 (114)
^{56}Fe	2_1^+ [a]	5.5	2.6	3.9	2.256 (19)	19.74 (64)	25.95 (3.40)
	2_1^+ [b]	5.9	3.1	4.4	2.280 (22)	19.49 (53)	26.07 (3.42)

[a] 130 MeV.
[b] 145 MeV.

where g is the g factor of the state of interest and B_{TF} is the transient field acting for the time $(t_{\mathrm{out}}-t_{\mathrm{in}})$ while the ions traverse the gadolinium layer; the exponential accounts for the decay of the excited state with lifetime τ.

The lifetimes of most excited states discussed above have been measured simultaneously using the DSAM technique with the 0° Ge detector. The high ion velocities (see Table I) implied high sensitivity for the lifetimes in the picosecond range. The Doppler broadened line shapes of the emitted γ-ray lines were fitted for the known reaction kinematics applying stopping powers [16] to Monte Carlo simulations including the second order Doppler effect as well as the finite size and energy resolution of the Ge detector. The feeding from higher states was taken into account. This feeding, however, was crucial only in case of the ^{46}Ti$(2_1^+ \rightarrow 0_1^+)$ transition where the 2_1^+ state was populated by the decay of the 3_1^- state. In all other cases, the feeding of 2_1^+ states in the decay of the 4_1^+ and 2_2^+ states had negligible effects on the 2_1^+ lifetimes. The computer code LINESHAPE [17] was used in the analysis. The high quality of the line-shape fits obtained is shown in Fig. 9. Characteristic differences in the slowing down of the ions in the different target layers giving rise to pronounced structures in the line shape were well reproduced. Relevant quantities extracted from all these measurements are summarized in Table I.

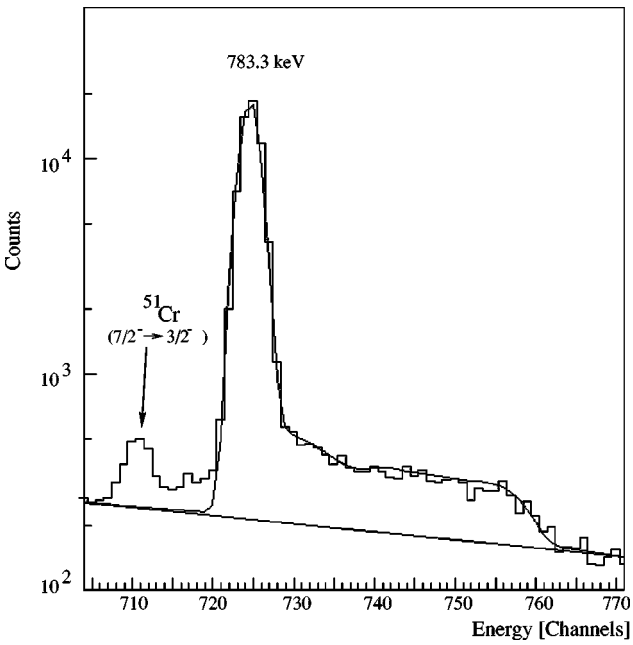

FIG. 9. Fit to the line shape of the ^{50}Cr $(2_1^+ \rightarrow 0_1^+)$ transition. The small peak corresponds to a transition in ^{51}Cr produced in a one-neutron transfer reaction.

III. RESULTS

The g factors were derived from the experimental precession angles, Φ^{expt}, by determining the effective transient field B_{TF} on the basis of the linear parametrization [18]:

$$B_{\mathrm{TF}}(v_{\mathrm{ion}}) = G_{\mathrm{beam}} \cdot B_{\mathrm{lin}} \tag{4}$$

with

$$B_{\mathrm{lin}} = a(Gd) \cdot Z_{\mathrm{ion}} \cdot \frac{v_{\mathrm{ion}}}{v_0}, \tag{5}$$

where the strength parameter $a(Gd) = 17(1)$ Tesla [18], $v_0 = e^2/\hbar$, and $G_{\mathrm{beam}} = 0.83(4)$ is the attenuation factor accounting for the dynamic demagnetization of the gadolinium induced by the ion beam [4,19]. The calculated precessions Φ^{lin}/g are listed for each nuclear state in Table I. The magnitude and dependence of the attenuation factor G_{beam} on relevant parameters such as stopping power and intensity of the beam ions as well as on the electron orbitals of the excited projectiles at their respective velocities were determined from the results of several experiments carried out under kinematical conditions very similar to those of the present work [19]. In fact, the mean stopping powers of the Ti and Cr beam ions in gadolinium were, at their respective energies, practically equal $\langle dE/dx \rangle \simeq 9$ MeV/μm. Moreover, the mean velocities of the excited ions in the ferromagnet (Table I) relative to the Bohr velocities in the $2s$ and $3s$ orbitals, $\langle v_{\mathrm{ion}}^{\mathrm{Ti,Cr}} \rangle / v_{2s}^{\mathrm{Bohr}} \simeq 0.45$ and $\langle v_{\mathrm{ion}}^{\mathrm{Ti,Cr}} \rangle / v_{3s}^{\mathrm{Bohr}} \simeq 1.4$ imply almost identical ion fractions in these ns-electron configurations relevant to the transient field strength (see also [18]). On the basis of the linear parametrization of the transient field and the well-established dependence of the attenuation

TABLE II. Measured lifetimes, deduced $B(E2)$'s, measured g factors, and full fp shell model (FSM) calculations for the 2_1^+ and 4_1^+ states in ^{46,48}Ti and ^{50,52}Cr.

Nucleus	State	τ [ps]		$B(E2\downarrow)$ [W.u.]		g factor	
		[20]	present	exp.	FSM	exp.	FSM
^{46}Ti	2_1^+	7.4 (6)	8.1 (4)	18.5 (9)	11.7	0.496(27)	0.285
	4_1^+	2.4 (2)	2.3 (2)	20.5 (18)	15.7	0.58(17)	0.244
^{48}Ti	2_1^+	6.2 (4)	5.7 (2)	15.0 (5)	9.1	0.392(19)	0.211
	4_1^+	1.8 (4)	1.1 (1)	18.4 (17)	13.7	0.54(13)	0.472
	2_2^+	0.059 (4)	0.073 (6)	5.5 (5)			
^{50}Cr	2_1^+	12.8 (7)	13.2 (4)	19.2 (6)	18.3	0.619(31)	0.568
	4_1^+	3.2 (4)	3.2 (7)	14.6 (32)	26.0	0.78(13)	0.742
^{52}Cr	2_1^+	1.02 (4)	1.13 (3)	10.3 (3)	12.4	1.206(64)	1.172
	4_1^+	1.5 (5)	9.6 $(^{+50}_{-24})$	10.3(34)	11.7		1.221

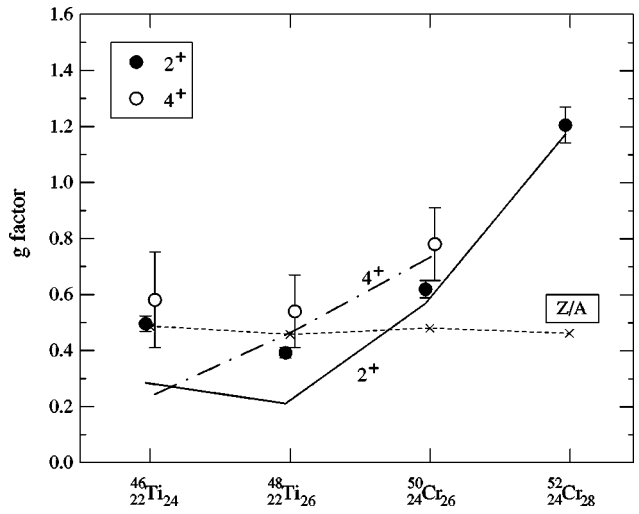

FIG. 10. Comparison of experimental g factors of the 2_1^+ and 4_1^+ states of Ti and Cr nuclei and full fp shell model calculations represented by solid and dotted–dashed lines. The dashed curve represents the value $g=Z/A$ predicted by the collective model.

factor G_{beam} on the stopping power of the beam ions and electron orbital velocity of the excited beam ions, the same value for G_{beam} is obtained for both Ti and Cr ions. The empirical parametrization [Eqs. (4) and (5)] was further checked with precession measurements on the first 2^+ state of ^{56}Fe with known g factor, $g=0.61(8)$ [5]. In these experiments, 130 MeV and 145 MeV ^{56}Fe ion beams were Coulomb excited on the same target in kinematic conditions similar to those pertaining to the Ti and Cr measurements (Table I). The analysis of the data yielded a mean attenuation factor $G_{\mathrm{beam}}=0.77(10)$, in good agreement with the adopted value. The final assigned error is mainly associated with the statistical uncertainty in the g factor measurement.

As seen in Table II, the uncertainty in the transient field strength contributes mainly to the error in $g(2_1^+)$, whereas the statistical error of the experimental precession angles dominates the uncertainty of the $g(4_1^+)$ results. Corrections to the 2_1^+ precessions due to feeding from the 4_1^+ states and to beam bending effects were negligibly small. The stray magnetic field along the path of the recoil ions was effectively shielded. Table II summarizes the g factors and the $B(E2)$'s derived from the measured lifetimes. It is noted that in most cases the newly determined lifetimes agree very well with earlier data. However, there are also significant differences between the present results and the values quoted in the literature, especially for ^{48}Ti(4_1^+) and ^{52}Cr(4_1^+). The present result for ^{52}Cr(4_1^+) agrees with that of a recoil distance measurement [20]. The sensitivity and reliability of the present experiments were substantially increased by the use of high ion velocities.

IV. DISCUSSION

The measured g factors and $B(E2)$'s were compared with the full fp shell model (FSM) calculations (Table II) carried out with the computer code ANTOINE [21] using a modified version of the Kuo-Brown effective interaction KB3 [22] in which the gap around ^{56}Ni is reduced and a density dependence is included [23]. It is noteworthy that the present calculations differ considerably from the earlier calculations [24] which used a drastically truncated model space due to the computer limitations.

The general trend of the precise $g(2_1^+)$ values shows a small but significant decrease from ^{46}Ti to ^{48}Ti and a subsequent rise towards ^{52}Cr, where the $N=28$ shell is closed. This behavior is well reproduced by the calculations, as shown in Fig. 10. The pattern observed is clearly associated with excitations of nucleons from the $0f_{7/2}$ orbit to the $1p_{3/2}$, $0f_{5/2}$, and $1p_{1/2}$ orbits which break the particle-hole symmetry of the cross-conjugate nuclei ^{46}Ti (two protons, four neutron holes) and ^{50}Cr (four protons, two neutron holes) [24]. The experimental and theoretical $B(E2)$'s are compared in Fig. 11. An increase of collectivity towards the lighter Ti nuclei is evident from the figure; the closing of the $N=28$ shell for ^{50}Ti and ^{52}Cr is reflected by small $B(E2)$'s.

The most interesting, and indeed surprising, results emerge when the full fp shell model calculations are compared with the new experimental data (Table II and Figs. 10

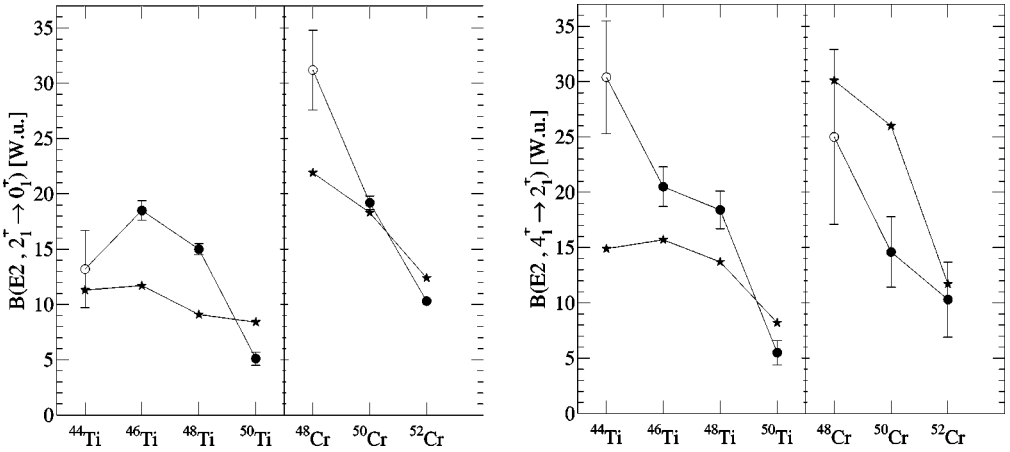

FIG. 11. Comparison of the experimental $B(E2)$'s (closed circle, present data; open circle [20]) and the results from full fp shell model calculations (asterisk). The lines are drawn to guide the eye.

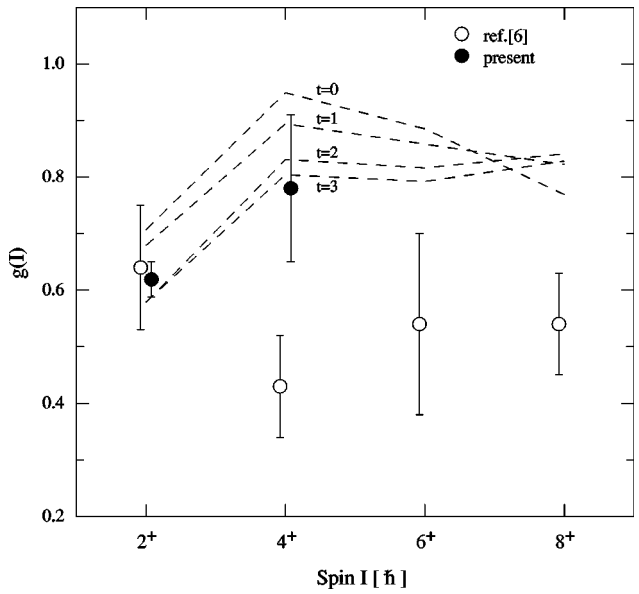

FIG. 12. Comparison of experimental g factors for ^{50}Cr with shell model calculations which allow t valence nucleons to lie outside the $0f_{7/2}$ shell [7].

and 11). In the upper half of the $f_{7/2}$ shell, the g factors and $B(E2)$'s of ^{50,52}Cr agree rather well with theory. The prediction that the g factors should be large is confirmed. The unexpected results show up when the theory is applied to ^{46,48}Ti. One might expect *a priori* that the full fp shell model calculations would better reproduce the collectivity of these nuclei. Hence, the KB3 interaction is likely deficient in this respect, and excitations of the ^{40}Ca core should be included. It has long been recognized that ^{40}Ca is not as good a closed shell nucleus as ^{48}Ca [25]. Furthermore, low-lying, highly deformed states in ^{40}Ca, ^{41}Ca, ^{42}Ca and other neighboring nuclei could admix into the 2_1^+ and 4_1^+ states of ^{46,48}Ti.

The importance of including the whole fp shell in the description of the structure of these nuclei is further put in evidence by the calculations of $g(I)$ for ^{50}Cr [7] in which an increasing number of t valence nucleons is excited from the $0f_{7/2}$ orbit to the other fp shell orbits using the KB3 interaction (Fig. 12). Evidently, the best agreement between theory and the present data is achieved for $t \geqslant 2$. The same conclusion has been drawn by Nakada *et al.* [26] and Caurier *et al.* [27,28] in their description of the structure of heavier fp shell nuclei. Figure 12 also displays the former g factor measurements in ^{50}Cr [6] which disagreed strongly with all existing microscopic calculations [7,8]. The striking discrepancy no longer exists for the new data. In the previous measurements the nuclear states were populated in a fusion reaction which generally implies a complex feeding pattern. Without knowing the precise time history of the feeding paths it is not possible to determine the precession of a particular nuclear state in which the nucleus finds itself during its traversal of the region of the target in which the transient field is effective. Only with the technique combining recoil distance and transient field can this problem be avoided [29]. This uncertainty, however, is absent in Coulomb excitation measurements.

V. SUMMARY AND CONCLUSIONS

As in the former measurements on Se nuclei [3], the technique of projectile Coulomb excitation in inverse kinematics allows high precision measurements of the g factors of the 2_1^+ states of Ti and Cr nuclei and, for the first time, of the g factors of the 4_1^+ states. In particular, the latter results emphasize the potential of the experimental technique. The accuracy of the $g(2_1^+)$ values is mainly determined by the uncertainty of the transient field parametrization, which, in the present case, was checked in a calibration measurement on a neighboring nucleus, ^{56}Fe with known g factor. It is noteworthy, that the *relative g* factors of several states of the different isotopes are free of this systematic uncertainty.

Although the data for low-lying states of the four fp shell nuclei studied show an overall agreement with full fp shell model calculations, there are surprisingly large deviations in the g factors of these states and the $B(E2)$ values of the corresponding transitions. Whereas the data for ^{50,52}Cr nuclei are in good agreement with theory, the experimental g factors for ^{46,48}Ti are closer to the collective value of Z/A. The observed deviations are attributed to shortcomings in the model which ignores possible excitations of the sd shell core. This lack of collectivity in the calculations is also observed in the $B(E2)$'s which systematically underestimate the experimental data.

The present paper shows the importance of high precision g factors which reveal fine details of the structure of short-lived nuclear states hardly recognizable in experiments with lower precision. The successful measurement of the g factors of the weakly excited 4_1^+ states gives confidence that the technique will be applicable to future experiments with radioactive beams of low intensity.

ACKNOWLEDGMENTS

The authors are indebted to A. Poves and H. Nakada for many stimulating discussions. We are thankful to the operators of the accelerators at Cologne and Munich for their assistance throughout the experiments. We also appreciate the collaboration of A. Aprahamian at the start of this work. Support by the BMBF, the Deutsche Forschungsgemeinschaft, and the U.S. National Science Foundation is acknowledged.

[1] J. Holden, N. Benczer-Koller, G. Jakob, G. Kumbartzki, T. Mertzimekis, K.-H. Speidel, P. Maier-Komor, A. Macchiavelli, M. McMahan, and W. Rogers (unpublished).

[2] G. Jakob, N. Benczer-Koller, J. Holden, G. Kumbartzki, T. Mertzimekis, K.-H. Speidel, C.W. Beausang, and R. Krücken, Phys. Lett. B **468**, 13 (1999); (unpublished).

[3] K.-H. Speidel, N. Benczer-Koller, G. Kumbartzki, C. Barton, A. Gelberg, J. Holden, G. Jakob, N. Matt, R.H. Mayer, M.

Satteson, R. Tanczyn, and L. Weissman, Phys. Rev. C **57**, 2181 (1998).
[4] R. Ernst, K.-H. Speidel, O. Kenn, U. Nachum, J. Gerber, P. Maier-Komor, N. Benczer-Koller, G. Jakob, G. Kumbartzki, L. Zamick, and F. Nowacki, Phys. Rev. Lett. **84**, 416 (2000).
[5] P. Raghavan, At. Data Nucl. Data Tables **42**, 189 (1989).
[6] A.A. Pakou, J. Billowes, A.W. Mountford, and D.D. Warner, Phys. Rev. C **50**, 2608 (1994).
[7] L. Zamick and D.C. Zheng, Phys. Rev. C **54**, 956 (1996).
[8] G. Martinez-Pinedo, A. Poves, L.M. Robledo, E. Caurier, F. Nowacki, J. Retamosa, and A. Zuker, Phys. Rev. C **54**, R2150 (1996).
[9] K.-H. Speidel, J. Cub, U. Reuter-Knopp, W. Karle, H. Busch, S. Kremeyer, J. Gerber, and F. Hagelberg, Z. Phys. A **342**, 17 (1992).
[10] P. Maier-Komor, K.-H. Speidel, and A. Stolarz, Nucl. Instrum. Methods Phys. Res. A **334**, 191 (1993).
[11] K. Alder, Helv. Phys. Acta **25**, 235 (1952).
[12] H. Frauenfelder and R. M. Steffen, in *Alpha-, Beta-, and Gamma-Ray Spectroscopy*, edited by K. Siegbahn (North-Holland, Amsterdam, 1965), Vol. 2.
[13] R. D. Gill, *Gamma-Ray Angular Correlations* (Academic, New York, 1975).
[14] K. Alder and A. Winther, *Electromagnetic Excitation* (North-Holland, Amsterdam, 1975).
[15] K.-H. Speidel, G. Jakob, H. Busch, U. Grabowy, A. Gohla, J. Gerber, and H. Trinkaus, Nucl. Instrum. Methods Phys. Res. B **122**, 84 (1997).
[16] F.J. Ziegler, J. Biersack, and U. Littmark, *The Stopping and Range of Ions in Solids*, Vol. 1 (Pergamon, Oxford, 1985).
[17] J.C. Wells and N.R. Johnson, program LINESHAPE, Feb. 1994, ORNL.
[18] K.-H. Speidel, U. Reuter, J. Cub, W. Karle, F. Passek, H. Busch, S. Kremeyer, and J. Gerber, Z. Phys. D: At., Mol. Clusters **22**, 371 (1991).
[19] G. Jakob, J. Cub, K.-H. Speidel, S. Kremeyer, H. Busch, U. Grabowy, A. Gohla, O. Jessensky, and J. Gerber, Z. Phys. D: At., Mol. Clusters **32**, 7 (1994), and references therein.
[20] L.K. Peker, Nucl. Data Sheets **68**, 271 (1993); T.W. Burrows, *ibid.* **68**, 1 (1993); **75**, 1 (1995); Huo Junde, *ibid.* **71**, 659 (1994); F. Brandolini *et al.*, Nucl. Phys. **A642**, 387 (1998).
[21] E. Caurier, code ANTOINE, Strasbourg, 1989.
[22] A. Poves and A.P. Zuker, Phys. Rep. **70**, 235 (1981).
[23] J. Sanchez-Solano, Ph.D. thesis, Madrid, 2000.
[24] A.A. Pakou, R. Tanczyn, D. Turner, W. Jan, G. Kumbartzki, N. Benczer-Koller, Xiao-Li Li, Huan Liu, and L. Zamick, Phys. Rev. C **36**, 2088 (1987).
[25] R.A. Ricci, in Proceedings of the Topical Conference on the Structure of $1f_{7/2}$ Nuclei, Legnaro, 1971, edited by R. A. Ricci, p. 1.
[26] H. Nakada, T. Sebe, and T. Otsuka, Nucl. Phys. **A571**, 467 (1994).
[27] E. Caurier, A.P. Zuker, A. Poves, and G. Martinez-Pinedo, Phys. Rev. C **50**, 225 (1994).
[28] E. Caurier, G. Martinez-Pinedo, F. Nowacki, A. Poves, J. Retamosa, and A.P. Zuker, Phys. Rev. C **59**, 2033 (1999).
[29] A. Jungclaus, C. Teich, V. Fischer, D. Kast, K.P. Lieb, C. Lingk, C. Ender, T. Härtlein, F. Köck, D. Schwalm, J. Billowes, J. Eberth, and H.G. Thomas, Phys. Rev. Lett. **80**, 2793 (1998).